**Proceedings of MSEC2006**
**2006 ASME International Conference on Manufacturing Science and Engineering**
**October 8-11, 2006, Ypsilanti, MI**

**MSEC2006-21004**

# EFFECT OF FLUENCE ON THE DISCOLORATION OF MARBLE CLEANED WITH UV LASERS

**Jie Zhang**
**Department of Mechanical Engineering**
**Columbia University**
**New York, NY 10027**
**jz2112@columbia.edu**

**Andrew J. Birnbaum**
**Department of Mechanical Engineering**
**Columbia University**
**New York, NY 10027**
**ajb2118@columbia.edu**

**Y. Lawrence Yao**
**Department of Mechanical Engineering**
**Columbia University**
**New York, NY 10027**
**yly1@columbia.edu**

## ABSTRACT

The effect of fluence level on the discoloration of marble surfaces after the removal of the encrustation by 355nm laser pulses is comparatively studied. Considering the thermochemical reaction possibly occurring in the encrustation during laser irradiation, the mechanism responsible for the discoloration of the cleaned marble surface is analyzed. The reduction of iron oxides by graphite plays a key role in determining the final color of the cleaned marble surface. A two-dimensional laser ablative cleaning model including the reaction heat is applied to calculate the temperature distribution during laser heating. The kinetics of the thermochemical reaction is estimated based on the simulated temperature field. The occurrence of the thermochemical reaction is also verified indirectly with experiments. The marble surfaces before and after laser irradiation are characterized in term of the chemical components through surface enhanced Raman spectroscopy. The surface color is measured with a chromameter using a 1976 CIE Lab color system. The proposed mechanism is also applied to numerically analyze the severer discoloration of marble cleaned with laser pulses at 1064nm.

## INTRODUCTION

Marble, a metamorphic limestone, primarily consists of calcite, a crystalline form of calcium carbonate ($CaCO_3$). Marble is widely used in statues and monuments, as well as a structural material. Its exposure to a sulphur dioxide ($SO_2$)-polluted atmosphere, particularly in an urban environment, results in a thin layer of black encrustation gradually developed on the marble surface sheltered from the water due to the formation of gypsum ($CaSO4{\cdot}2H2O$). Sulphur dioxide from the combustion of fossil fuels readily reacts with the $CaCO_3$ present in the marble to form gypsum. The softer and more water-soluble gypsum is easily contaminated by soot particles containing metal oxide and graphite, as well as numerous organic constituents, further contributing to the generation of the black encrustation [1].

This encrustation has a detrimental effect on the aesthetic value of of both artistic and practical marble structures. Moreover, the encrustation facilitates the biodeterioration of the marble since it can host to bacteria, lichen, mosses, higher plants and other microorganisms [2]. Chemical cleaning is of the traditional means for removing the encrustation. However, there exists the possibility of chemical reactions between the utilized chemical agents and marble, as well as the environmental pollution. The encrustation is also mechanically removed through using a scalpel or the air-abrasive machine. The effectiveness of the scalpel is restricted by the restorative talents of the restorer and the brittleness of the material. The results of air-abrasive machine treatments are also largely dependent on the restorer's skill levels, as the machine can not distinguish the encrustation from the stone. Due to the non-

uniformity of the encrustation, unavoidable surface damage of the marble results in the loss of fine details of the artworks [3].

Pulsed lasers removal of the encrustation is a promising alternative due to the fast and non-contact operation and the high-precision spatial and temporal control. In addition, the laser pulses can not damage the marble surface after the removal of the encrustation due to the large difference in the absorptivity between the encrustation and the marble, which is termed a self-limiting [3]. Laser cleaning nano-particles from semiconductor surfaces [4] and surface layer from metals or semiconductors [5] have been extensively studied. Since the pulsed laser cleaning of the encrustation from the marble was first implemented by John Asmus in 1971[6], massive investigations related to the laser cleaning of stoneworks have been performed.

Laboure et. al. [7] explored the effect of laser fluence, spot area, and water spraying on the cleaning rate of the stone. Siano et. al. [8] studied how pulse duration affects the laser stone-cleaning process. Siano et. al. [9] also experimentally determined the fluence thresholds corresponding to the various side effects in laser stone cleaning. LIBS (Laser-induced Breakdown Spectroscopy) was employed as an in-situ technique for monitoring the laser removal of the encrustation by Maravelaki et. al. [10]. Rodriguez-Navarro et. al. [11] found that the marble surface got roughening by the excessive laser pulses at supposedly safe fluence levels.

Both Maravelaki-Kalaitzaki et. al. [12] and Marakis et. al. [13] comparatively investigated the removal of different types of encrustation with different wavelengths. While the prominent self-limiting at 1064 nm is extremely beneficial in protecting the marble surface, the cleaned marble surface becomes severely yellowing. On the contrary, no severely yellowing occurs on the marble surface cleaned at 355 nm.

Klein et. al. [14] and Potgieter-Vermaak et. al. [15] both postulated that the yellowing at 1064 nm is due to the residues of iron oxides on the marble surface detected by their conducted experiments. However, they did not provide any explanation for the presence of these residues. Zafiropulos et. al. [16] proposed that the discoloration is mainly an optical phenomenon. The dark particles are vaporized by the IR laser fluences below the cleaning threshold to generate the voids in the encrustation. These voids make the light scattering different so that the color perception is altered towards yellow. Nevertheless, this argument falls short of evidences.

In the present paper, the influence of the fluence levels on the surface color of marble cleaned with the 355nm laser pulses is examined. A mechanism leading to the discoloration of the marble surface is proposed based on the analysis of the thermochemical reactions possibly occurring in the encrustation during laser irradiation. A two-dimensional laser ablative cleaning model including the reaction heat of the thermochemical reactions is applied in simulating the temperature field generated by the laser irradiation. Then, the kinetics of the thermochemical reactions is used to verify their presence. The proposed mechanism is also used to explain the severe discoloration of marble cleaned with laser pulses at 1064nm.

## EXPERIMENT CONDITIONS

A Q-switched Nd:YAG laser operating at 355 nm in $TEM_{00}$ mode is used as the light source. The laser has a pulse duration of 50 ns, with a constant repetition rate at 1 kHz. The beam diameter is set at 100 μm and the pulse fluence is varied from 0.3 J/cm$^2$ to 3 J/cm$^2$ through adjusting the distance of the sample from the focusing lens.. The sample is placed on the computer-controlled XYZ stage in open air, while the compressed air blows on the sample to prevent the ablation-formed plasma from touching the focusing lens during the experiment.

Italian white Carrara marble is selected as the investigated sample with dimensions 15mm×15mm×9mm. Its surface is honed to eliminate the obvious surface dents. The sample is thoroughly cleaned with the methanol before making the encrustation. For the numerical calculation of the laser produced temperature field in the marble, the encrustation is artificially made to better control the material property. The encrustation is a compound of 5% or 10% hematite ($Fe_2O_3$) powder, 20% graphite powder and 75% or 70% gypsum ($CaSO_4 \cdot 2H_2O$) (vol. %), mixed with the distilled water, and smeared onto the marble with the brush [14]. The marble with the encrustation is then left for 72 hours in a storage box. On average, the encrustation thickness is approximately 120 micron.

## RELATED THERMOCHEMICAL REACTIONS

### *Thermal dehydration and decomposition of gypsum ($CaSO_4 \cdot 2H_2O$)*

Gypsum ($CaSO_4 \cdot 2H_2O$, calcium sulfate dehydrate), the major ingredient in the encrustation, is a crystalline mineral that contains about 21% chemically combined water by weight. When the gypsum is heated, two endothermic dehydration reactions and one decomposition reaction occur successively. At the temperature of 373K, the first thermal dehydration reaction called calcinations occurs as follows [17]:

$$CaSO_4 \cdot 2H_2O \rightarrow CaSO_4 \cdot \frac{1}{2} H_2O + \frac{3}{2} H_2O - 17.2 \text{ kJ/mol} \quad (1)$$

This reaction is complete by 433K. Then, as the temperature rises to 573K, the second dehydration reaction begins to occur as:

$$CaSO_4 \cdot \frac{1}{2} H_2O \rightarrow CaSO_4 + \frac{1}{2} H_2O - 8.6 \text{ kJ/mol} \quad (2)$$

During these two reactions, the water is released as steam with an absorbed energy of 81.7 kJ/mol. Therefore, the total required energy in the dehydration of gypsum is 107.5 kJ/mol.

At temperatures above 1373K, calcium sulfate ($CaSO_4$) starts to decompose into calcium oxide (CaO) and sulfur dioxide ($SO_2$) according to the following equation [18]:

$$CaSO_4 \rightarrow CaO + SO_2 - 480\ kJ/mol \quad (3)$$

Calcite ($CaCO_3$) is dissociated into CaO and carbon dioxide ($CO_2$) starting at the temperature of 1173K to 1223K [19]. The reaction is described as the follows,

$$CaCO_3 \rightarrow CaO + CO_2 - 170\ kJ/mol \quad (4)$$

### *Hematite reduced by solid carbon*

When a mixture of hematite ($Fe_2O_3$) and solid carbon is heated up to the certain temperature, the hematite is reduced into wustite (FeO) at an extremely high rate through two consecutive steps, namely hematite → magnetite ($Fe_3O_4$) → wustite, like $Fe_2O_3(s) + C(s) \rightarrow 2FeO(s) + CO$ [20]. Then, two coupled gas-solid reactions take place,

$$FeO + CO \rightarrow Fe + CO_2 \quad (5)$$
$$CO_2 + C \rightarrow 2CO \quad (6)$$

It is known that the reaction (5) is catalysed by the reduced metallic iron. More carbon monoxide (CO) produced in the vicinity of FeO increases the reduction rate of FeO.

If the molten hematite is reduced by solid carbon, the reduction rate rises rapidly. This is termed a smelting reduction. The possible reason is that the molten FeO can more easily contact carbon than solid FeO [21]. The weight volume of FeO is proportional to its reduction rate by solid carbon due to the increased interface area between FeO and carbon [22]. Also, CaO even at the low concentration can significantly expedite this reduction reaction [20]. The catalysis results from the enhanced formation rate of CO through the following redox process,

$$CaO + CO_2 \rightarrow CaO{\cdot}O + CO \quad (7)$$
$$CaO{\cdot}O + C \rightarrow CaO + CO \quad (8)$$

The above introduced thermochemical reactions are summarized in Fig.1. During the laser heating, these thermochemical reactions may occur in the encrustation when the encrustation temperature reaches the reaction-required temperature, since temperature is one of most important factors, such as concentration, pressure, surface area and so on, leading to the occurrence of chemical reactions..

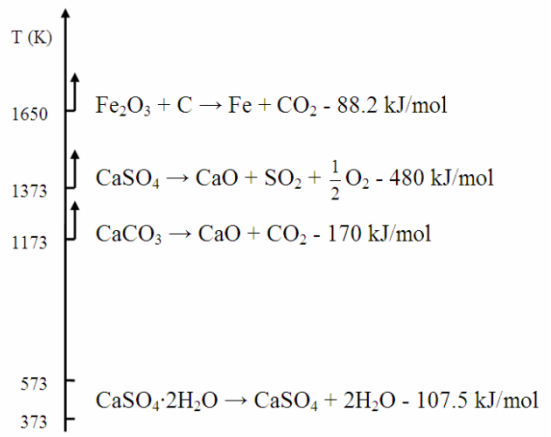


**FIG. 1 SUMMARY OF THERMOCHEMICAL REACTIONS OCCURING IN THE LASER-IRRADIATED ENCRUSTATION**

## NUMERICAL SIMULATION

Laser removal of the encrustation from the marble surface is based on laser ablation. Zhang and Yao [5] presented a two-dimensional laser ablative cleaning model which considers the discontinuity across the Knudsen layer and Stephen Boundary at the interface. Through the enthalpy method, the temperature field can be simulated and the resulting phase interfaces identified. In the present paper, the heats of thermochemical reactions occurring in the encrustation are taken into account in the model. When the materials reach the required temperature for the thermochemical reaction, the corresponding reaction heat is integrated into the energy balance equation as:

$$\frac{\partial h}{\partial t} + \frac{\partial \Delta H}{\partial t} = \frac{\partial}{\partial x}(\alpha \frac{\partial h}{\partial x}) + \frac{1}{r}\frac{\partial}{\partial r}(r\alpha \frac{\partial h}{\partial r}) \quad (9)$$

where α is heat diffusivity, $x$ and $r$ are the coordinates along the thickness and radial direction. The enthalpy of the material (heat content of the material) $H$ is expressed as $H = h + \Delta H$, where the sensible heat, $h = c_p T$ ($c_p$ is specific heat, $T$ is temperature), and $\Delta H$ is the latent heat of phase change $\Delta H_P$ or the reaction heat $\Delta H_T$.

The reaction rate is assumed to follow Arrhenius law, $k = k_0 \exp(-\frac{E}{RT})$, where $k_0$ is the frequency factor, $E$ is the activation energy, $R$ is the universal gas constant, $T$ is the temperature. Concerning reactions (1), (2), (3) and (4), the corresponding incorporated reaction heats are calculated as $\Delta H_T = k\Delta H_{T0}$, where $\Delta H_{T0}$ is the reaction heat. The FeO melting point of 1650 $K$ is assumed to be the separation point of the application ranges of two reaction rates. In addition, since the mechanism of reaction (5) and (6) is complicated by the co-existence of $Fe_2O_3$, FeO and Fe, a volume-reaction model is applied in their kinetic analysis [23]. It is assumed that reaction rates follow the first-order kinetic equation,

$$\gamma_{Fe_2O_3} = -k_1[Fe_2O_3] \quad (10)$$

$$\gamma_{FeO(s)} = 2k_1[Fe_2O_3] - k_2[FeO(s)] \quad (T_p \prec 1650K) \quad (11)$$

$$\gamma_{FeO(l)} = 2k_1[Fe_2O_3] - k_2[FeO(l)] \quad (T_p \geq 1650K) \quad (12)$$

$$\gamma_{Fe(sorl)} = k_2[FeO(s)] + k_3[FeO(l)] \quad (13)$$

Total reaction heat is computed like

$$\Delta H_T = \Delta H_1 \cdot \gamma_{Fe_2O_3} + \Delta H_2 \cdot \gamma_{FeO(s)} + \Delta H_3 \cdot \gamma_{FeO(l)} \quad (14)$$

where $\Delta H_1$, $\Delta H_2$, $\Delta H_3$ are the corresponding reaction heat.

The material parameters of the encrustation are the mass-averaged value of every component. All of the material properties are from [24]. The calculation domain is chosen as 3 times the beam diameter in both the radial and depth direction. The sample-absorbed fluence is assumed to be $F = (1-R) f e^{-(r/b)^2}$, where $b$ is laser beam radius, $f$ is incident fluence, $R$ is reflectivity of sample surface.

## MATERIAL CHARACTERIZATIONS

The chromameter (Minolta CR-300) is employed to measure the surface color of the marble. In principle, light reflected from the measured surface is simultaneously collected by three photocells, each with spectral sensitivities equal to one of the color matching functions of a special CIE standard observer. The CR-300 has a measurement spot diameter of 8mm and use D56 standard xenon light to irradiate the surface. The color measurements are expressed in the perceptually uniform color space, CIE L*a*b* (CIELAB), shown in Fig. 2. The $L^*$ axis is known as the lightness ranging from 0 (black) to 100 (white). The $a^*$ axis and $b^*$ axis represent redness-greenness and yellowness-blueness, respectively. Total color difference $\Delta E_{ab}$ is defined as, $\Delta E_{ab} = \sqrt{(\Delta L)^2 + (\Delta a)^2 + (\Delta b)^2}$, where $\Delta L = L - L_t$ describes the lightness change, $\Delta a = a - a_t$ and $\Delta b = b - b_t$ describe the chromaticity change, $L_t$, $a_t$, and $b_t$ are values of reference white [25].

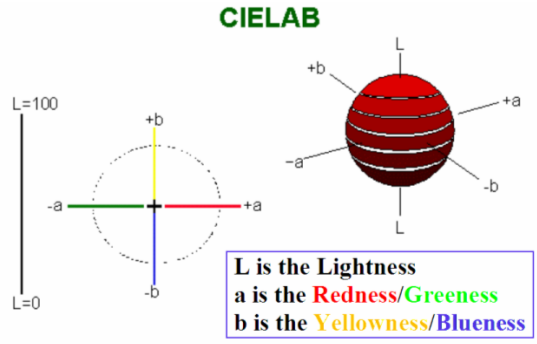


**FIG. 2 SCHEMATIC OF A 1976 CIE-LAB COLOR SYSTEM**

Surface enhanced Raman spectroscopy (SERS) is used to detect the chemical constituents of the marble surface. When the molecule is shined by a photon with energy differing from the energy discrepancy between its two stationary energy levels, the immediately occurring stokes Raman scattering reveals its structural information. The Raman signals from the surface are largely enhanced by the silver colloids smeared on the surface. The small silver particles allow the excitation of its localized surface plasmon. The resultant electromagnetic energy density is the primary contributor to the enhancement observed in SERS [26]. Raman spectra are excited using a 514 nm CW Argon-ion laser (Spectra-Physics model 2020) at a power of approximately 20 mW. The scattered lines are collected at 90° with a Spex model 1401 double monochromator (resolution ca. 2 $cm^{-1}$) and detected by an ITT FW-130 photomultiplier (PM) tube with Raman 2005 (software package).

Scanning Electron Microscopy (JEOL) and Scanner (HP Scanjet 5100C) are employed to take the images of cleaned marble surface, respectively. In the case of SEM, the marble surface should be coated with silver so that it is electrically conductive.

## RESULTS AND DICUSSIONS

### *Determination of fluence threshold*

The successful cleaning is defined as the complete removal of the encrustastion without any change of the marble surface in the integrity, structure and color. To experimentally determine the fluence threshold, the sample is irradiated by a single pulse per location. The fluence is continuously increased. When the damage of the encrustation including 5% hematite or the marble is noticeable under the optical microscope, the corresponding fluence values are considered as the thresholds. The experimentally determined threshold for the encrustation and the marble are 0.45 $J/cm^2$ and 2.5 $J/cm^2$, respectively.

In order to estimate the accuracy of the proposed numerical model, the fluence threshold is also determined with this model. At 50 ns, the fluence increasing the encrustation surface to the mass-averaged value of the graphite vaporization temperature, the decomposition temperature of hematite and gypsum, namely 2160 K, is considered as its threshold. Similarly, the fluence heating the marble surface to the decomposition temperature of calcite is the threshold for the marble. In figure 3, the Raman spectrum of the marble has four bands of $CaCO_3$ at 158, 285, 711 and 1084 $cm^{-1}$. It is evident that the principal ingredient of the marble is $CaCO_3$.

The numerically determined thresholds are 0.3 $J/cm^2$ and 1.8 $J/cm^2$ for the encrustation and the marble, respectively. If the model does not include the thermochemical reaction heat, the determined threshold is 0.12 $J/cm^2$ and 0.42 $J/cm^2$ for the encrustation and the marble, respectively. The thresholds determined by the model with the reaction heat are more close to the experimental ones, which shows this model is accurate to some extent. The slight overestimate of the model in the laser-induced-thermal field is possibly because the heat taken away by the released gases produced in the thermochemical reactions

is neglected in the model. Both the experimental and numerical results demonstrate that the threshold difference between the encrustation and the marble is large. This provides the marble cleaning at 355 nm for the self-limiting thereby avoiding damaging the marble substrate.

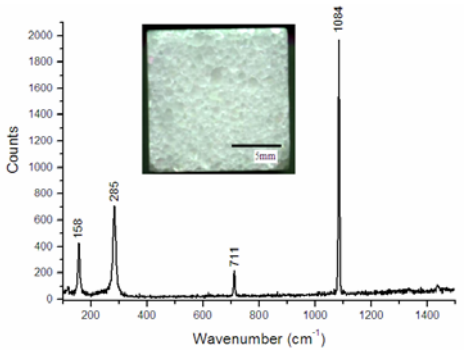


**FIG. 3 RAMAN SPECTRUM AND IMAGE OF WHITE CARRARA MARBLE**

### *Effect of fluence levels*

*Experiments*

Under the multiple-pulse strategy, the applied laser fluence should be higher than the encrustation threshold of 0.45 J/cm2 and lower than the marble threshold of 2.5 J/cm2. Here, the laser fluence is chosen as 0.67 J/cm$^2$ and 1.3 J/cm$^2$, respectively. Considering the chromameter measurement spot diameter of 8 mm, a circular encrustation area with the diameter of 9 mm is removed. The laser pulses irradiate the encrustation along the circular orbits from the outside to the inside. The pulses have the overlapping rate of 50% to reduce the effect of the Gaussian beam on the irradiation results.

The samples with the encrustation containing 5% hematite are employed in the experiments. Figure 4 (a) and (b) are the scanned images of the marble cleaned by 8 pulses at 0.67 J/cm$^2$ and 5 pulses at 1.3 J/cm$^2$, respectively. The color measurements of the original and cleaned marble surface as well as the encrustation are listed in Table 1. In Fig. 4 (c), the color measurements are shown in the 1971 Lab color space. All of color data is the average of 5 independent measurements.

**Table 1 COLOR MEASUREMENTS**

| | Original marble | Encrustation | Marble cleaned at 0.67 J/cm$^2$ | Original marble | Encrustation | Marble cleaned at 1.3 J/cm$^2$ |
|---|---|---|---|---|---|---|
| ΔL | 90.8433 | 59.39 | 84.2767 | 88.2367 | 59.39 | 86.1133 |
| Δa | -1.0333 | 11.2167 | -0.20333 | -1.19 | 11.2167 | -0.58333 |
| Δb | -0.94 | 13.9633 | 1.89333 | -0.8967 | 13.9633 | -0.0333 |

ΔL: Lightness; Δa: Red-Green; Δb: Blue-Yellow

Compared with the original marble surface, the lightness of the encrustation is much lower, which indicates the black appearance of the encrustation due to the graphite. The positive values of Δa and Δb denote the encrustation color is inclined to the redness and yellowness owing to the dark-brown hematite in the encrustation.

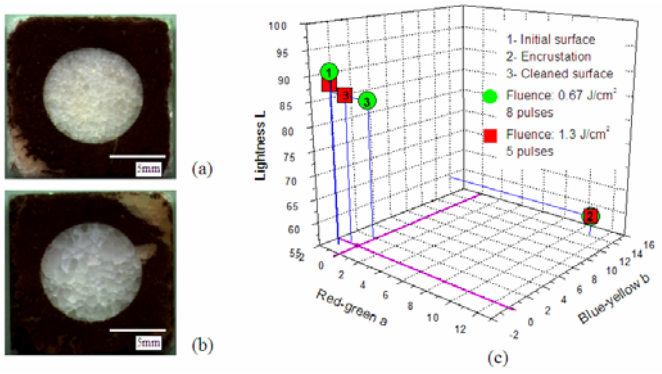


**FIG. 4 IMAGES AND COLOR MEASUREMENTS OF THE MARBLE SURFACES CLEANED WITH DIFFERENT FLUENCE LEVELS (a) 0.67 J/cm$^2$ (b) 1.3 J/cm$^2$**

The lightnesses of both cleaned marble surfaces are very close to the original ones, which implies the removal of the encrustation. However, the lightness difference between the cleaned and the original surfaces is larger in the case of 0.67 J/cm$^2$. This reflects the encrustation may not be completely removed. At 1.3 J/cm$^2$, both of Δa and Δb are close to the original values and have the same sign. It can be concluded that there is no color variation. At 0.67 J/cm$^2$, Δa is close to the original one and has the same sign. However, Δb has the positive sign, which means the surface is becoming slightly yellowing. This phenomenon is referred to as the discoloration of the marble surface.

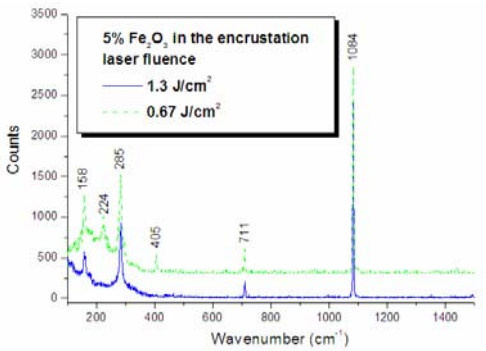


**FIG. 5 RAMAN SPECTRUM OF MARBLE SURFACES CLEANED WITH DIFFERENT FLUENCE LEVELS**

The Raman spectra of two cleaned surfaces are shown in Fig. 5. The spectrum of the surface irradiated at 1.3 J/cm$^2$ only has the bands of $CaCO_3$ at 158, 285, 711, 1084 cm$^{-1}$. Yet, the spectrum of the surface irradiated at 0.67 J/cm$^2$ consists of bands of $CaCO_3$ and bands of $Fe_2O_3$ at 224 and 405 cm$^{-1}$. The $CaCO_3$ bands in two spectra indicate the marble surfaces are exposed after the removal of the encrustation. The $Fe_2O_3$ bands reflect $Fe_2O_3$ still resides on the surface irradiated at 0.67 J/cm$^2$. Thus, it could be deduced that the presence of $Fe_2O_3$ is related to the surface discoloration. Very few $Fe_2O_3$ on the white

calcite surface may result in a yellow shift [27]. The SEM pictures of these two cleaned marble surfaces are shown in Fig. 6. Some particles are on the surface cleaned at 0.67 J/cm$^2$. The surface cleaned at 1.3 J/cm$^2$ is fairly clean.

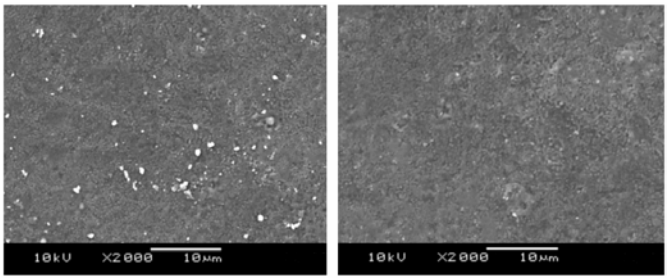


(a) (b)

**FIG. 6 SEM IMAGES OF MARBLE SURFACES CLEANED WITH TWO FLUENCE LEVELS (a) 0.67 J/cm$^2$ (b) 1.3 J/cm$^2$**

*Analysis of the discoloration mechanism*

*The Hematite reduced by the graphite*

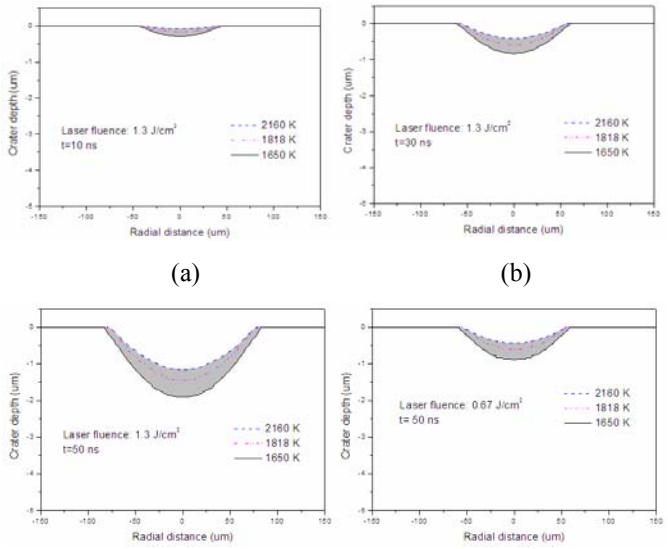


(a) (b)

(c) (d)

**FIG. 7 SIMULATED TEMPERATURE DISTRIBUTION PRODUCED BY DIFFERENT FLUENCE LEVELS (a) 1.3 J/cm$^2$ at 10 ns (b) 1.3 J/cm$^2$ at 30 ns (c) 1.3 J/cm$^2$ at 50 ns (d) 0.67 J/cm$^2$ at 50 ns**

Figure 7 shows the simulated history of temperature distribution in the encrustation produced at 1.3 J/cm$^2$ and the temperature distribution at 50ns induced by the fluence of 0.67 J/cm$^2$. $Fe_2O_3$ and FeO in the grey area are in the molten state due to the temperature ranging between the melting point of $Fe_2O_3$ 1818 K and the one of FeO 1650 K. Some graphite powder may contact the molten $Fe_2O_3$ and FeO because of their random distribution in the encrustation. Correspondingly, part of the molten iron oxides may be reduced by the graphite to produce iron at the very high reaction rate. As mentioned before, this reduction reaction can be considerably accelerated by CaO from the thermal dissociation of $CaSO_4$. In the case of 1.3 J/cm$^2$, the grey area emerges starting from 10 ns, and is enlarged with the time, which means the smelting reduction of iron oxides may take place during the entire 50 ns. At 0.67 J/cm$^2$, the grey area at 50 ns suggests the availability of the temperature required by this reaction.

The simulated distribution of Fe, FeO and $Fe_2O_3$ at 50ns with the fluence of 0.67 J/cm$^2$ and 1.3 J/cm$^2$ is shown in Fig. 8. The iron is generated in both cases. The higher the fluence is, the more metallic iron is produced. The evident reason is that the high temperature induced by the high fluence favors the reduction of iron oxides. It should be pointed out that very little hematite is reduced by graphite and the majority of the hematite is ablated by the laser pulse.

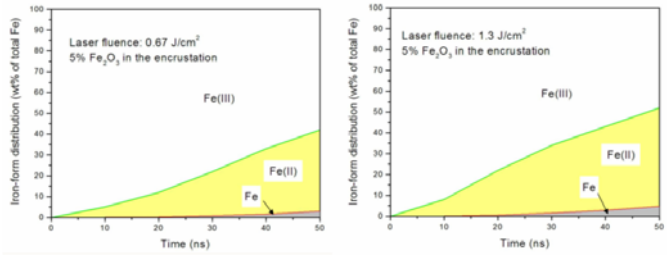


(a) (b)

**FIG. 8 SIMULATED IRON-FORM DISTRIBUTION AT 50ns INDUCED BY TWO FLUENCE LEVELS (a) 0.67 J/cm$^2$ (b) 1.3 J/cm$^2$**

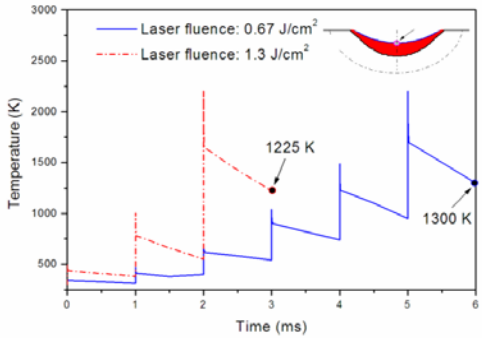


**FIG. 9 SIMULATED TEMPERATURE HISTORY AT THE FINAL CRATER BOTTOM CENTER OF THE ENCRUSTATION**

Figure 9 describes the temperature history at the bottom center of the crater generated by 3 pulses at 1.3 J/cm$^2$ and 6 pulses at 0.67 J/cm$^2$. In the case of 0.67 J/cm$^2$, iron oxides are heated above 1000 K by 3 pulses, respectively. The longer reaction time of the solid iron oxides reduced by the graphite at the high temperature may result in the production of more iron. On the contrary, only one pulse can heat the material above 1000 K in the case of 1.3 J/cm$^2$. Also, heat accumulation between two successive pulses is enhanced with the pulse

number. After 3 pulses at 1.3 J/cm$^2$, the temperature is 1225 K; after 6 pulses at 0.67 J/cm$^2$, the temperature is 1300 K.

*The reduced metallic iron during laser irradiation* During the laser irradiation, the formed plasma impedes the air from interacting with the surface. The dissociation of the ablated hematite in the plasma will produce the atomic oxygen [28]. However, oxygen has no solubility in liquid iron, preventing the production of iron oxide at this step [29]. Yet, Pereira et. al. [30] experimentally found that the apparition of a $Fe_2O_3$ layer at the iron surface after the irradiation of the XeCl laser. This means that the formation of $Fe_2O_3$ is due to the chemical reaction between iron and oxygen during the cooling stage. The chemically active iron reacts easily with the oxygen, especially at high temperatures. Since the formation enthalpy of iron oxide is small, iron oxides are produced very near the surface. The iron oxides is a multilayer scale consisting of FeO, $Fe_3O_4$ and $Fe_2O_3$ from the iron bulk to the outermost [31]. Increases in the time that the iron is subjected to high temperatures can lead to increases in the production of iron species in a higher oxidation state, i.e., more $Fe_2O_3$ is formed.

The majority of iron produced by the current pulse may be taken away by the vaporization flux during the next pulse, and the rest of the iron may be ablated by subsequent pulses, or is just melted and resides on the encrustation. The following investigation focuses on the iron irradiated by the last pulse required by the complete removal of the encrustation, namely the 7$^{th}$ pulse at 0.67 J/cm$^2$ and the 4$^{th}$ pulse at 1.3 J/cm$^2$. It is assumed an independent iron particle is irradiated by a single pulse. The 2-D ablation model is employed to simulate the temperature distribution in iron [32]. The reflectivity of iron at 355 nm is 0.58 [24]. Considering the heat accumulation, the initial temperature of iron is set as 1225 K and 1300 K, as shown in Fig. 9, with the fluence of 1.3 J/cm$^2$ and 0.67 J/cm$^2$, respectively.

In the case of 1.3 J/cm$^2$, the temperature in a crater with the depth of 0.22 μm is simulated to be equal or higher than the vaporization point of iron 3134 K, which means the iron is ablated. Though the actual thickness of the iron left on the marble is difficult to measure, it is certainly relatively minute. Thus, it can be assumed that all of the iron has been ablated. In the case of 0.67 J/cm$^2$, no iron is simulatedly heated up to 3134 K. The temperature above the melting point of iron 1811 K is in the crater with the depth of 0.4 μm. Thus, the iron is assumed to be just melted.

The simulated temperature history of the points corresponding to the beam center at the different depths in the case of 0.67 J/cm$^2$ is shown in Fig. 10. It is apparent that the peak temperature is generated at the end of the pulse. The iron could be oxidized during its cooling period of approximately 1s. Due to the high temperature in the very shallow iron, the iron oxides is in the form of $Fe_2O_3$.

When the iron is melted by the low fluence pulse, the molten iron may penetrate the porous structure of the marble surface. As extra pulses incident on the marble, the marble surface temperature is raised very slightly due to its low absorptivity. At this time, the hematite is heated mainly through heat conduction from the marble. Thus, the temperature of hematite may be much lower than its vaporization temperature.

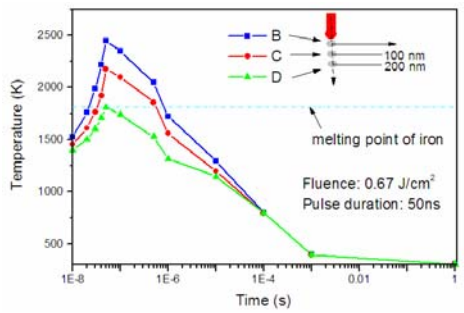


**FIG. 10 SIMULATED TEMPERATURE HISTORY AT THE LOCATION CORRESPONDING TO THE BEAM CENTER ON THE IRON SURFACE**

*Effect of graphite*

Without graphite, the encrustation consists of 5% hematite and 95% gypsum. The encrustation is irradiated by 8 pulses at 0.67 J/cm$^2$ and 5 pulses at 1.3 J/cm$^2$, respectively. The color of original and cleaned marble surfaces as well as the encrustation are measured and listed in Table 2, respectively.

**Table 2 COLOR MEASUREMENTS**

| | Original marble | Encrustation | Marble cleaned at 0.67 J/cm$^2$ | Original marble | Encrustation | Marble cleaned at 1.3 J/cm$^2$ |
|---|---|---|---|---|---|---|
| ΔL | 86.5633 | 66.8067 | 85.09 | 87.0067 | 66.8067 | 85.67 |
| Δa | -1.2933 | 20.6333 | -0.8 | -1.057 | 20.6333 | -0.25 |
| Δb | -0.7633 | 10.9733 | -0.21 | -0.85 | 10.9733 | -0.1933 |

ΔL: Lightness; Δa: Red-Green; Δb: Blue-Yellow

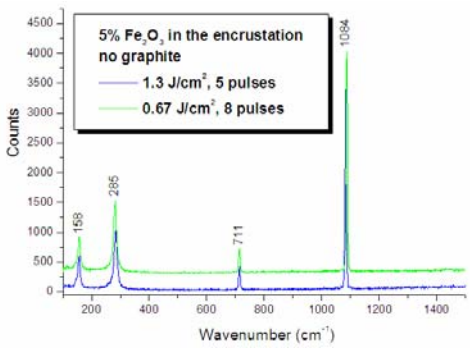


**FIG. 11 RAMAN SPECTRUM OF MARBLE SURFACE AFTER THE REMOVAL OF THE ENCRUSTATION WITHOUT THE GRAPHITE WITH DIFFERENT FLUENCE LEVELS**

In the case of two fluence levels, the lightness of cleaned surface is very close to its corresponding original value. Meanwhile, two lightness differences between the cleaned and the original surface are almost equal. This probably means the

encrustation is completely removed in both cases. Both of Δa and Δb values are also close to the original ones, and the signs are identical. So, it can be concluded that there is no color variation on the marble surface cleaned at 0.67 J/cm$^2$ and 1.3 J/cm$^2$. The Raman spectra measured on these two cleaned surfaces are shown in Fig. 11. Both of two Raman spectra are characterized with the bands of $CaCO_3$ (158, 285, 711 and 1084 cm$^{-1}$). No $Fe_2O_3$ bands of 224 and 405cm$^{-1}$ appear. This indicates no $Fe_2O_3$ exists on two cleaned marble surface. Without the graphite, the hematite in the encrustation is just heated, and then ablated. This group of experiments indirectly verifies the hematite is reduced by the graphite to produce iron during laser irradiation.

### *Effect of volume weight of hematite*

Marble samples are covered with the encrustation containing 10% hematite, 20% graphite, and 70% gypsum. These samples are also irradiated by 8 pulses at 0.67 J/cm$^2$ and 5 pulses at 1.3 J/cm$^2$, respectively. Table 3 lists the color measurements of original and cleaned marble surfaces as well as the encrustation, respectively.

**Table 3 COLOR MEASUREMENTS**

| | Original marble | Encrustation | Marble cleaned at 0.67 J/cm$^2$ | Original marble | Encrustation | Marble cleaned at 1.3 J/cm$^2$ |
|---|---|---|---|---|---|---|
| ΔL | 89.3667 | 57.4067 | 82.0667 | 88.2867 | 57.4067 | 86.51 |
| Δa | -1.3067 | 19.0167 | -0.49667 | -1.2833 | 19.0167 | -0.68933 |
| Δb | -1.79 | 13.4667 | 2.99333 | -1.0533 | 13.4667 | 0.03 |

ΔL: Lightness; Δa: Red-Green; Δb: Blue-Yellow

The color variation of the surfaces cleaned at 0.67 J/cm$^2$ and 1.3 J/cm$^2$ is similar to the corresponding color measurements shown in section 6.2.1. The only difference is the value of Δb after the irradiation of the pulse at 0.67 J/cm$^2$. It further shifts towards the positive direction, which means the yellowing of the cleaned surface is aggravated.

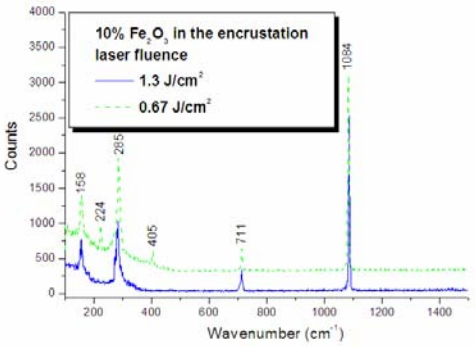


**FIG. 12 RAMAN SPECTRUM OF MARBLE SURFACE AFTER THE REMOVAL OF THE ENCRUSTATION WITH 10% HEMATITE WITH DIFFERENT LASER FLUENCE LEVELS**

Figure 12 shows the Raman spectra collected from these two cleaned surfaces. Both samples have the $CaCO_3$ bands of 158, 285, 711 and 1084 cm$^{-1}$. Only the sample irradiated at 0.67 J/cm$^2$ shows the $Fe_2O_3$ bands of 224 and 405 cm$^{-1}$, which indicates the presence of $Fe_2O_3$ on the marble surface irradiated at 0.67 J/cm$^2$.

The increased yellowing shift is probably due to the high volume weight of hematite in the encrustation. Lee, et. al. [22] found that the reduction rate of hematite by graphite rises with the weight of hematite owing to the augmentation of the interface area between hematite and graphite. Therefore, increase iron production results in an increase in the formation of iron oxides. Such experimental results indicate the occurrence of the thermochemical reaction to some extent.

### *Analysis of severely yellowing of marble at 1064 nm*

In order to explain the severely yellowing of marble cleaned at 1064 nm with the proposed mechanism, the experimental parameters applied in [14] are adopted in the following analysis. The artificial encrustation contains 20% graphite, 20% hematite, and 60% gypsum. The encrustation is removed by 10 or 20 pulses at 0.5 J/cm$^2$. The pulse duration is 7 ns, and the repetition rate is 2 Hz. In the simulation, the beam size is assumed to be 100 μm in diameter, and the encrustation thickness is 120 μm. The properties of the encrustation are recalculated based on the new ratio of the ingredients.

Figure 13 shows the simulated temperature distribution in the encrustation generated with a fluence of 0.5 J/cm$^2$ at 7 ns. The ablation temperature of this encrustation is assumed to be 2250 K. Clearly, the temperature in part of the encrustation is in the range from 1818 K (melting point of $Fe_2O_3$) to 1650 K (melting point of FeO). The smelting reduction of hematite by graphite may take place to form the iron in this area.

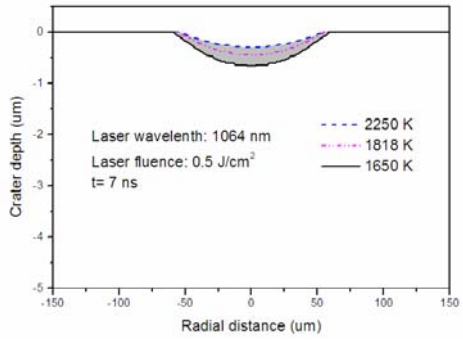


**FIG. 13 SIMULATED TEMPERATURE DISTRIBUTION IN THE ENCRUSTATION PRODUCED BY A 1064 nm LASER PULSE**

Whether iron can be ablated by the last applied pulse in the experiment is related to the final presence of iron on the surface. Therefore, an independent iron particle is assumed to be irradiated by the 10th pulse and the 20th pulse at 0.5 J/cm2, respectively. The absorptivity of iron at 1064 nm is around 0.31 [24]. Similarly, the initial temperature of iron is numerically calculated to be 700K and 1150K in the case of the 10$^{th}$ pulse and the 20$^{th}$ pulse, respectively. The simulated temperature

history of the point corresponding to the beam center at the iron surface is shown in Fig. 14. In both cases, the peak temperature is lower than the vaporization temperature of iron 3134 K, which means the iron can not be ablated, just melted. After the pulse is over, the iron requires almost one second to cool. Then, the oxygen can react on the high temperature iron to form iron oxides. Hence, the marble surface gets yellowing. The severely yellowing at 1064 nm may result from the generation of more iron oxide as well. Since both the marble and the iron absorptivities at 1064 nm are low, it is unlikely that the iron will be ablated. However, the marble absorptivity at 355nm is slightly higher. The marble-absorbed heat may be helpful in increasing the temperature of the iron to its vaporization point, and hence reducing the amount of the remaining iron.

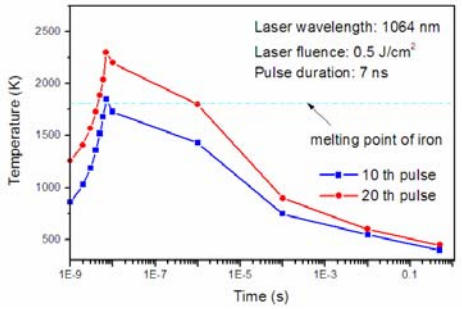


**FIG. 14 SIMULATED TEMPERATURE HISTORY AT THE LOCATION CORRESPONDING TO THE BEAM CENTER ON THE IRON SURFACE INDUCED BY A PULSE AT 1064 nm**

## CONCLUSIONS

The fluence levels affect the surface color of marble after the removal of the encrustation by 355nm laser pulses. During laser irradiation, some hematite may be reduced by the graphite to produce iron. The iron may be ablated with the high fluence, and left on the marble surface with the low fluence. The iron oxides from the oxidation of the remaining iron may be responsible for the light discoloration of the marble surface cleaned with the low fluence. The laser-induced temperature field is calculated with a two-dimensional laser ablative cleaning model including the reaction heat to analyze the kinetics of the thermochemical reactions. With the low fluence, the removal of the encrustation without the graphite does not cause any discoloration to the marble, which indirectly verifies the occurrence of the reduction reaction of hematite. The higher the volume weight of hematite in the encrustation, the more yellow the marble surface becomes, which implies an increase in the volume weight of hematite increases the reduction rate of hematite. The severe discoloration of marble cleaned at 1064nm may be due to the inability to ablate the iron produced in the reduction of hematite.

## ACKNOWLEDGMENTS

The authors are grateful to Prof. John Lombardi of CCNY and Dr. Mohammad Athar of Columbia University for their permission to access the Raman spectroscopy and the chromameter, respectively. And, the authors thank Ms. Fen Xu and Mr. Justin Rasso for their technical assistance during these measurements.

## REFERENCES

[1] Skoulikidis, T, and Charalambous, D., 1981, "Mechanism of Sulphation by Atmospheric $SO_2$ of the Limestones and Marbles of the Ancient Monuments and Statues, II. Hypothesis Concerning the Rate Determining Step in the Process of Sulphation, and Its Experimental Confirmation," British Corrosion Journal, **16**, pp. 49-55.

[2] Griffin, P. S., Indictor, N., and Koestler, R. J., 1991, "The Biodeterioration of Stone: a Review of Deterioration Mechanisms, Conservation Case Histories, and Treatment," International Biodeterioration, **28**, pp. 187-207.

[3] Cooper, M., 1998, Laser Cleaning in Conservation: An Introduction, Butterworth-Heinemann.

[4] Tam, A. C., Leung, W. P., Zapka, W., and Ziemlih, W., 1992, "Laser-cleaning Techniques for Removal of Surface Particulates," J. Appl. Phys., **71**(7), pp. 3515-3523.

[5] Zhang, J., Wang, Y., Cheng, P., and Yao, Y. L., 2006, "Effect of Pulsing Parameters on Laser Ablative Cleaning of Copper Oxides," J. Appl. Phys., 064902.

[6] Asmus, J. F., Munk, W., and Murphy C., 1974, "Studies on the Interaction of Laser Radiation with Art Artifacts," Proceedings of the Society of Photo-Optical Instrumentation Engineers, **v 4**, pp. 19-27.

[7] Laboure, M., Bromblet, P., Orial, G., Wiedemann, G. and Simon-Boisson, C., 2000, "Assessment of Laser Cleaning Rate on Limestones and Sandstones," J. Cult. Herit., **1**, pp. s21-s27.

[8] Siano, S., Margheri, F., Pini, R., Mazzinghi, P., and Salimbeni, R., 1997, "Cleaning Processes of Encrusted Marbles by Nd:YAG Lasers Operating in Free-running and Q-switched Regimes," Appl. Opt., **36**(27), pp. 7073-7079.

[9] Siano, S., Fabiani, F., Pini, R., Salimbeni, R., Giamello, M., Sabatini, G., 2000, "Determination of Damage Thresholds to Prevent Side Effects in Laser Cleaning of Pliocene Sandstone of Siena," J. Cult. Herit., **1**, pp. s47-s53.

[10] Maravelaki, P., Zafiropulos, V., Kilikoglou, V., Kalaitzaki, M., and Fotakis, C., 1997, "Laser-induced Breakdown Spectroscopy as a Diagnostic Technique for the Laser Cleaning of Marble," Spectrochim. ACTA Part B, **52**, pp. 41-53.

[11] Rodriguez-Navarro, C., Rodriguez-Navarro, A., Elert, K., and Sebastian, E., 2004, "Role of Marble Microstructure in

Near-infrared Laser-induced Damage during Laser Cleaning," J. Appl. Phy., **95**(7), pp. 3350-3357.

[12] Maravelaki-Kalaitzaki, P., Zafiropulos, V., and Fotakis, C., 1999, "Excimer Laser Cleaning of Encrustation on Pentelic Marble: Procedure and Evaluation of the Effects," Appl. Surf. Sci., **148**, pp. 92-104.

[13] Marakis, G., Pouli P., Zafiropulos, V., and Maravelaki-Kalaitzaki, P., 2003, "Comparative Study on the Application of the 1st and 3rd Harmonic of a Q-switched Nd:YAG Laser System to Clean Black Encrustation on Marble," J. Cult. Herit., **4**, pp. 83s-91s.

[14] Klein, S., Fekrsanati, F., Hildenhagen, J, Dickmann, K., Uphoff, H., Marakis, Y., and Zafiropulos, V., 2001, "Discoloration of Marble during Laser Cleaning by Nd:YAG Laser Wavelengths," Appl. Surf. Sci., **171**, pp. 242-251.

[15] Potgieter-Vermaak, S., Godoi, R., Grieken, R., Potgieter, J., Oujja, M., and Castillejo, M., 2005, "Micro-structural Characterization of Black Crust and Laser Cleaning of Building Stones by Micro-Raman and SEM Techniques," Spectrochim. ACTA Part A, **61**, pp. 2460-2467.

[16] Zafiropulos, V., Balas, C., Manousaki, A., Marakis, Y., Maravelaki-Kalaitzaki, P., Melesanaki, K., Pouli, P., Stratoudaki, T., Klein S., Hildenhagen, J., Dickmann, K., Luk'Yanchuk, B., Mujat, C., and Dogariu, A., 2003, "Yellowing Effect and Discoloration of Pigments: Experimental and Theoretical Studies," J. Cult. Herit., **4**, pp. 249s-256s.

[17] Mehaffey, J. R., Cuerrier, P., and Carisse, G., 1994, "A Model for Predicting Heat Transfer through Gypsum-Board/Wood-Stud Walls Exposed to Fire," Fire and Materials, **Vol. 18**, pp. 297-305.

[18] Fuertes, A., and Fernandez, M., 1995, "Kinetics of the Calcium Sulphate Decomposition," Trans IchemE, **73**, Part A, pp. 854-862.

[19] Lipinski, W., and Steinfeld, A., 2004, "Heterogeneous Thermochemical Decomposition under Direct Irradiation," Int. J. Heat Mass Trans., **47**, pp. 1907-1916.

[20] Jagtap, S. B., Pande, A. R., and Gokarn A. N., 1991, "A Model for Reduction of Hematite by Carbon: Evaluation of the Catalytic Role of Calcium Salt," J. Chem. Eng. Japan, **25**(1), pp. 6-10.

[21] Sato, A., Aragane, G., Kamihara, K., and, Yoshimatsu, S., 1987, "Reduction Rate of Molten Iron Oxide by the Solid Carbon or the Carbon in Molten Iron," Tetsu-to-Hagane, **73**, pp. 812-819.

[22] Lee, J., Min, D., and Kim, S., 1997, "Reaction Mechanism on the Smelting Reduction of Iron Ore by Solid Carbon," Metallurg. Mater. Trans. B, **Vol. 28B**, pp. 1019-1028.

[23] Sugawara, K., Morimoto, K., and Sugawara, T., 1999, "Dynamic Behavior of Iron Forms in Rapid Reduction of Carbon-coated Iron Ore," AIChE J., **45**(3), pp. 574-580.

[24] Lide, D. R., 2004-2005, CRC Handbook of Chemistry and Physics, CRC Press, Boca Raton, FL.

[25] Berns, R., 2000, Billmeyer and Saltzman's Principles of Color Technology, John Wiley & Sons Inc., NewYork.

[26] Ferraro, J., 2003, Introductory Raman Spectroscopy, Academic Press, Boston.

[27] Barro′n, V., and Torrent, J., 1986, "Use of the Kubelka-Munk theory to study the influence of iron oxides on soil colour," J. Soil Sci., **37**, pp. 499-510.

[28] Pereira, A., Delaporte, P., Sentis, M., Cros, A., Marine, W., Basillais, A., Thomann, A., Leborgne, C., Semmar, N., Andreazza, P., and Sauvage, T., 2004, "Laser Treatment of a Steel Surface in Ambient Air," Thin Solid Films, **453-454**, pp. 16-21.

[29] Schaaf, P., Han, M., Lieb, K., and Carpene, E., 2002, "Laser Nitriding of Iron with Laser Pulses from Femtosecond to Nanosecond Pulse Duration," Appl. Phys. Lett., **80(**6), pp. 1091-1093.

[30] Pereira, A., Cros, A., Delaporte, P., Marine, W., and Sentis, M., 2002, "XeCl Laser Treatment of Steel Surface," Appl. Surf. Sci., **197-198**, pp. 845-850.

[31] Khanna, A. S., 2002, Introduction to High Temperature Oxidation and Corrosion, ASM International, Materials Park.

[32] Zhang, W. W., Yao, Y. L., and Chen, K., 2001, "Modelling and Analysis of UV Laser Micromachining of Copper," Int. J. Adv. Manuf. Technol., **18**, pp. 323-331.

 